



ORIGINAL ARTICLE

The anti-angiogenesis and antioxidant activity of chitosan-mediated synthesized selenium-gold nanostructure



Hoda Zarharan^a, Mahlasadat Bagherian^a, Ali Shah Rokhi^a,
Romina Ramezani Bajgiran^a, Ehsan Yousefi^b, Pedram Heravian^a,
Mitra Niazi Khazrabig^a, Ali Es-haghi^{a,*}, Mohammad Ehsan Taghavizadeh Yazdi^{c,*}

^a Department of Biology, Mashhad Branch, Islamic Azad University, Mashhad, Iran

^b Department of Cell and Molecular Biology & Microbiology, Faculty of Biological Science and Technology, University of Isfahan, Isfahan, Iran

^c Applied Biomedical Research Center, Mashhad University of Medical Sciences, Mashhad, Iran

Received 4 September 2022; revised 9 March 2023; accepted 10 March 2023

Available online 22 March 2023

KEYWORDS

Nanocomposites;
Chitosan;
AuNPs;
Selenium;
Anti-angiogenesis

Abstract A novel nanocomposite containing selenium-gold-chitosan (Se-Au-CS) was prepared and characterized using powder X-ray diffraction (XRD), Fourier transforms infrared spectroscopy (FTIR), UV-Vis spectroscopy, field emission scanning electron microscopy (FESEM), energy dispersive X-ray analysis (EDX) and transmission electron microscopy (TEM). The powder X-ray diffraction has shown successful synthesis of Se nanoparticles. To further study the presence of gold nanoparticles, EDX and UV-Vis were used. The morphological studies and grain sizes have revealed polyhedral shapes with a mean particle size of ≈ 211 nm. The TEM images also indicated the presence of nanoparticles in the CS coating. The Anti-oxidant effects of Se-Au-CS were evaluated using the DPPH (2,2-diphenyl-1-picrylhydrazyl) assay. Moreover, in the chorioallantoic membrane (CAM) assay, notable anti-angiogenesis effects were observed for Se-Au-CS. The results of this study demonstrated effective anti-angiogenesis effects of Se-Au-CS were evaluated using CAM assay for the first time. It also indicated the application of Se-Au-CS could be extended to the treatment of various cancer diseases.

© 2023 The Author(s). Published by Elsevier B.V. on behalf of King Saud University. This is an open access article under the CC BY-NC-ND license (<http://creativecommons.org/licenses/by-nc-nd/4.0/>).

* Corresponding authors.

E-mail addresses: ashaghi@gmail.com (A. Es-haghi), taghavizadehme971@mums.ac.ir, metyazdi@gmail.com (M.E. Taghavizadeh Yazdi).
Peer review under responsibility of King Saud University.



1. Introduction

Nanotechnology showed a promising future in the treatment of cancer by increasing the drug efficacy and reducing side effects along with designing individualized drugs for targeting specific cancer cells in vivo and in vitro (Ghorani-Azam, 2022; Mobaraki, 2022; Shakerimanesh, 2022; Yazdi et al., 2020). One of the profound nanomaterials used in biology known for their anticancer properties is metallic-base ones, which have demonstrated intriguing properties as bioactive agents and drug carriers (Javad Farhangi, 2021; Mousavi-Kouhi, 2021; Alabyadh, 2022). Among synthetic methods to prepare metallic nanoparticles, using green methods highlighted that are based on economic indicators associated with price and availability (Es-haghi, 2021; Modarres and Yazdi, 2021; Amiri et al., 2021; Mohammadzadeh, 2022). In addition, its eco-friendliness is another prominent advantage of the green synthetic methods (Taghavizadeh Yazdi, 2022; Seyedi, 2023). Chitosan (CS) is a stabilizing agent and non-toxic material used in the preparation of metallic nanoparticles, which is extracted from natural sources and is one of the most used and safe natural biopolymers in drug manufacturing which can stabilize nanoparticles. Additionally, particles with a positive surface charge could also be drawn to the negative surface of the cell membrane (Asghar, 2021; Hashemzadeh, 2021; Mohamed, 2021). In absence of a suitable stabilizer, the Van der Waals forces between bare metallic nanoparticle would lead to aggregation. In contrast, CS is a steric barrier that surrounds the metal with a positive charge, generating homogeneous nanoparticle solutions thanks to strong electrostatic repulsion (Phan, 2021).

Selenium is a bioactive element and an important micronutrient for cell growth (Radomska, 2021; Rana, 2021), and selenoproteins modulate the cellular oxidation and reduction environment, immune system and toxicities (Labunskyy et al., 2014; Forceville, 2022) which is needed to be in the dietary foods to prevent the advent of possible related diseases including cancer (Evans et al., 2017; Qi, 2022). Due to its non-toxicity, biocompatible attributes and activities in the body are a safer choice as a base element to synthesize biocomposites that are active against cancer (Mangiapani et al., 2014; Raich, 2001; Rataan, 2022; Hashemzadeh, 2022; Hojjati Fard, 2022). Although selenium nanoparticles (SeNPs) have shown anticancer properties, their bioactivity could be improved significantly if modified with other metallic nanomaterials that have also proven to be effective against cancer (Malinga et al., 2021; Mirzaei, 2021; Jurj, 2017). Among nanomaterials to enhance the anticancer effects of selenium nanoparticles, gold nanoparticles (AuNPs) are safe, effective and biocompatible (Kang, 2020; Mousavi-Kouhi, 2021; Mobaraki, 2021). Therefore, using AuNPs as a modifier to enhance the anticancer properties of SeNPs can be of value to be investigated in a cellular model. Herein, selenium-gold-chitosan (Se-Au-CS) nanocomposite was synthesized and was analyzed structurally along with the functional groups, morphology and solid phase particle sizes.

Angiogenesis, which is the process of new blood vessel formation is necessary to human biology, and also plays a critical character in some pathologies such as tumor formation, metastasis, and ischemia (Lai, 2016; Ashna, 2020). Therefore, one of the tumor treatment strategies that leads to the destruction of tumor growth and inhibition of metastasis is anti-angiogenic agents (Teleanu, 2019). In this study, we synthesize Se-Au-CS, which has shown anti-oxidant and strong anti-angiogenic properties.

2. Experimental and materials

The materials were acquired from Sigma-Aldrich (USA). Chitosan (medium molecular weight) with 75–85% deacetylated was used. The XRD was performed with Cu k_{α} (1.54 Å) from 5° to 80°, FTIR was measured between 400 and 4000 m^{-1} (KBr pellets), FESEM (Mira 3 TESCAN) and TEM (Leo

912) were used to analyze morphology and size. UV-Visible spectrophotometry (PerkinElmer) to measure how much a chemical substance absorbs light.

2.1. Synthesis of Se-Au-CS

Selenium nanoparticles were synthesized according to the literature and modified for the preparation of the Se-Au-CS (Bai, 2017). In brief, solubilized sodium selenite (0.8 g) in water (20 mL) was added dropwise to the CS (1 g) and ascorbic acid (AC, 3.2 g) in a 1% (w/w) acetic acid solution (200 mL) while an ultrasound wave with the power of Q500 sonicator (750 W, 20 kHz). The stable red color indicated the successful synthesis of SeNPs in CS. To prepare Se-Au-CS, soluble AC (1.6 g) in water (20 mL) was added to the SeNPs solution and then, $H AuCl_4$ in water (20 mL the ratio of Se: Au was 100:3) was added dropwise to the previous solution. A grayish-red color was obtained. The solution of the Se-Au-CS was centrifuged and washed with double distilled water several times, then lyophilized and used without no further process for analyses and biological tests. Sedimentation studies have shown the nanoparticles were at least stable in solution for at least a month. After that, it appears the sedimentation of the nanoparticles occurs.

2.2. Chorioallantoic membrane (CAM) assay

CAM assays have been extensively employed for angiogenesis and metastasis analysis. In this way, the chicken chorioallantoic membrane was used to study the effect of Se-Au-CS on angiogenesis. For this purpose, 40 Ross-fertilized eggs were obtained from Tous Company and were transferred to the laboratory. In the laboratory, the eggs were sterilized with 70% alcohol and transferred to an incubator. After that, on day

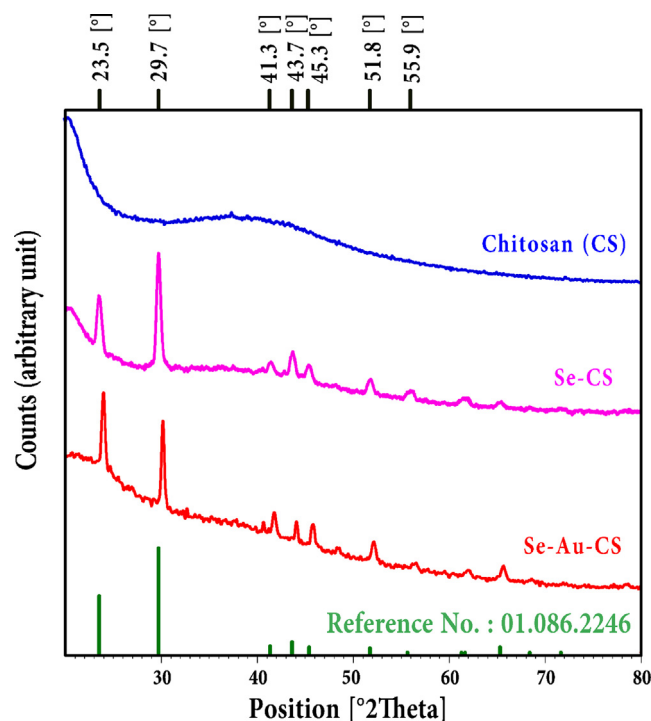


Fig. 1 The XRD pattern of chitosan (CS), Se-CS and Se-Au-CS.

4, a window was carved on each of the egg shells, and afterward, the carved windows were blocked with special glue, and the eggs were returned to the incubator. 8 days later, the windows were open again and a sterile sponge was placed on the chorioallantoic membrane. Finally, the sponges were treated

with nanoparticles. The windows were closed again, and the eggs were returned to the incubator for 4 more days. On day 12, for investigating the effects of Se-Au-CS on angiogenesis, the samples were investigated using a stereo microscope in terms of length and number of blood vessels and were analyzed using Image J software.

Table 1 The d-spacing, 2theta and intensity percentage value of the reference.

No.	h	k	l	d [Å]	2Theta[deg]	I [%]
1	1	0	0	3.78	23.50	47.90
2	1	0	1	3.01	29.68	100.00
3	1	1	0	2.18	41.31	14.60
4	0	1	2	2.07	43.62	27.40
5	1	1	-1	2.00	45.34	18.90
6	2	0	0	1.89	48.07	2.10
7	2	0	1	1.77	51.68	16.00
8	0	0	3	1.65	55.56	4.50
9	1	1	-2	1.64	56.08	8.20
10	0	1	3	1.51	61.15	3.40
11	0	2	2	1.50	61.63	7.90
12	1	2	0	1.43	65.20	9.60
13	2	1	-1	1.37	68.21	3.30
14	1	1	-3	1.32	71.54	3.20
15	3	0	0	1.26	75.31	0.10
16	0	2	3	1.24	76.48	0.60
17	2	1	-2	1.24	76.92	2.00
18	0	3	1	1.22	78.15	3.10

2.3. The antioxidant capacity of Se-Au-CS

The antioxidant capacity of NPs was evaluated by DPPH assay as explained by Rajamanikandan (Rajamanikandan, 2011). Briefly, a DPPH working solution (1 mg DPPH/10 mL methanol) and serial dilutions of NPs were prepared. Then, 500 μ L DPPH solution was added to an equal volume of various concentrations of NPs. The resulting solution was incubated in the dark at 30 $^{\circ}$ C for 30 min. Subsequently, the absorbance of samples was evaluated at 517 nm. Glutathione was employed as a positive control (Rajamanikandan, 2011). The inhibition of DPPH free radicals was evaluated by the following formula:

$$(\%) \text{ of inhibition} = \frac{(\text{Absorbance}_{\text{Control}} - \text{Absorbance}_{\text{Test}})}{(\text{Absorbance}_{\text{Control}})}$$

2.4. Cytotoxicity assay

Human umbilical vein endothelial cells (HUVEC) was selected as a suitable in vitro model. HUVEC cells were achieved from

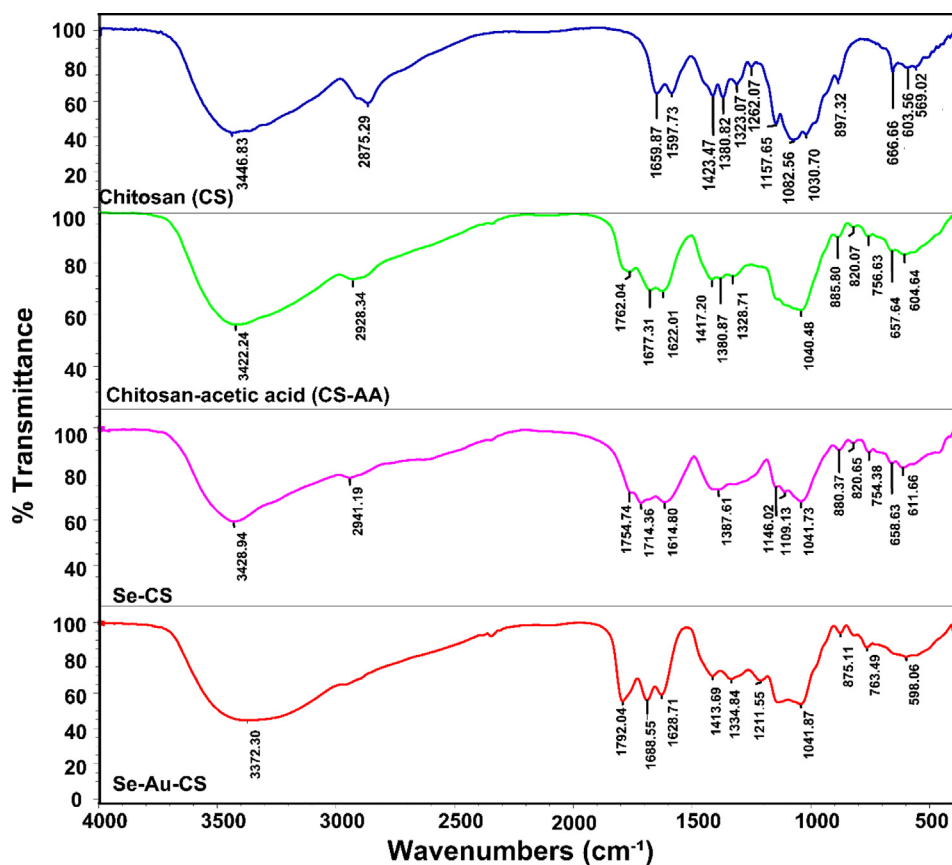


Fig. 2 The FTIR of the chitosan (CS), chitosan-acetic acid (CS-AA), Se-CS and Se-Au-CS.

Pasteur Institute, Iran. The cytotoxicity effects of NPs against HUVEC cells were evaluated by the MTT test. The cells were seeded in 96-well plates and incubated at 37 °C for 24 h. Then, the cells were treated with various concentrations (0, 31, 62.5, 125, 250, and 1000 µg/mL) of NPs. After that, 100 µL of MTT solution (0.45 mg/mL) was added to each well. Lastly, the absorption of the samples was recorded at 570 nm and the cell sustainability was assessed.

3. Results and discussion

3.1. The powder X-ray diffraction (XRD)

The chitosan (CS), Se-CS, Se-Au-CS were structurally investigated using the XRD (Fig. 1). The CS could have a broad peak in the range of 10–40° which revealed itself in the background in the Se-CS and Se-Au-CS (Julkapli et al., 2010). The metallic particles show specific patterns associated directly with their structure microscopically. The analyses due to low concentration AuNPs only revealed the SeNPs' related pattern which was compatible with JCPDS# 01.086.2246. Structurally, the crystal system and the space group of SeNPs were hexagonal

and P3121 respectively. The reference values of 2theta were 23.5, 29.7, 41.3, 43.6, 45.3, 48.1, 51.7, 55.6, 56.1, 61.1, 61.6, 65.2, 68.2, 71.5, 75.3, 76.5, 77.0, and 78.2° (Table 1). The experimental values showed a good agreement with the ones

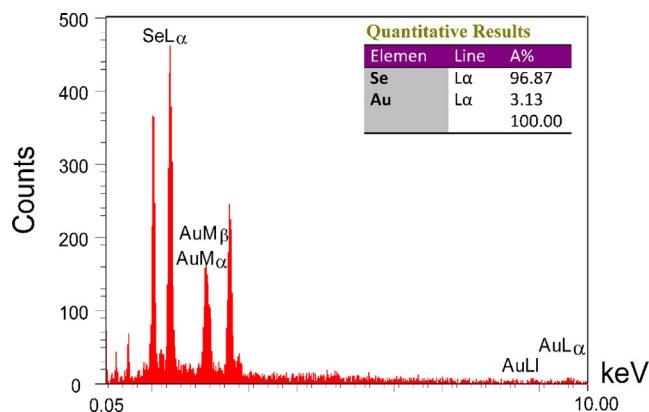


Fig. 4 The EDX analysis of Se-Au-CS.

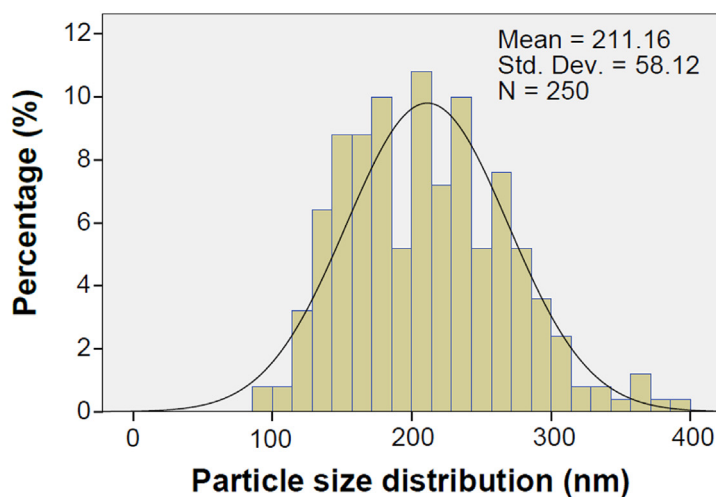
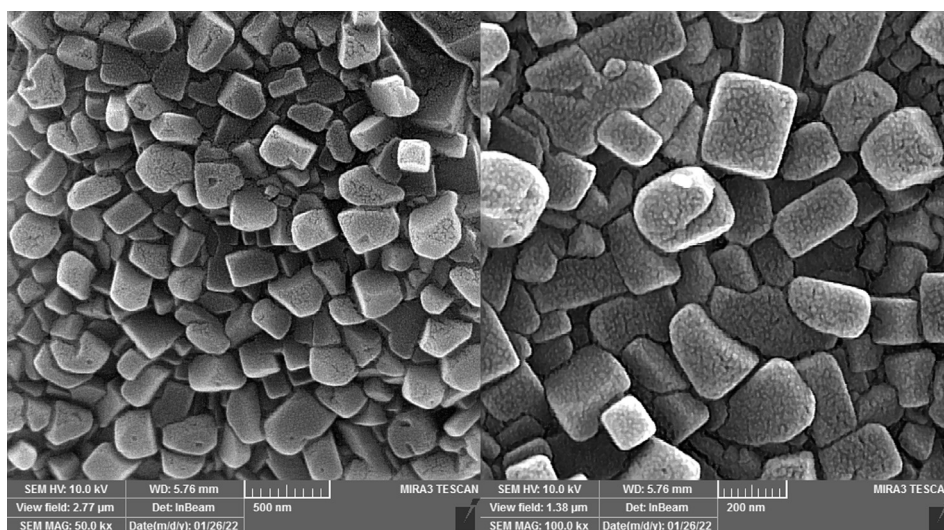


Fig. 3 The FESEM and particle size distribution of Se-Au-CS.

of the reference. Accordingly, the HKLs of the prepared samples were the same as the ones for the reference shown in Table 1. The analysis also showed the prepared Se nanoparticle in Se-CS and Se-Au-CS were a pure phase in its selenium part, but no trace of gold was presented in the patterns.

3.2. Fourier transforms infrared spectroscopy (FTIR)

The FTIR analyses of chitosan (CS), chitosan-acetic acid (CS-AA), Se-CS and Se-Au-CS were applied to assigning the presented functional groups in the composition that were related to the CS (Fig. 2). To prepare the samples for FTIR analysis, the as prepared solutions of CS, Se-CS and Se-Au-CS were dried overnight in an oven at 50 °C and KBr pellets were used. The CS showed a characteristic band at 3422 cm^{-1} associated with hydroxyl stretching. The bare selenium and gold nanoparticles show no specific bands. Hence, only the changes in the functional groups of the organic residues were explained in detail (Selvapriya, 2022; Seol, 2013). The band at 2898 cm^{-1} was C–H stretching of CS. The amid I, amide II and amide III bands of CS were observed at 1659 cm^{-1} , 1597 cm^{-1} and 1323 cm^{-1} respectively. The stretching and bending of CH_2 also appeared at 1423 and 1380 cm^{-1} . The band at 1157 cm^{-1} and 1082 were ascribed to the vibrations of C–O–C and pyranose structure (Singh and Dutta, 2009). The use of acetic acid (AA) to make the CS solution could lead to the appearance of new peaks after drying. The presence of acetic acid in FTIR of solubilized chitosan is a common phenomenon that could explain the presence of the new bands at 1762, 1754 and 1794 cm^{-1} in FTIR of chitosan-acetic acid (CS-AA), Se-CS and Se-Au-CS respectively (Frick, 2021; Colomer, 2013). The broad absorption bands with a peak at 3428 and 3372 cm^{-1} showed the presence of hydroxyl and amine groups in the nanocomposite. It appears that the C–H stretching associated with CS also appeared in the region between ≈ 2850 to ≈ 2950 cm^{-1} . Therefore, the introduced Se-Au-CS nanocomposite contained a trace amount of AA in its composition. In fact, AA could form a stable acid base pair with chitosan, which could be accounted for its presence even

after drying. Another possibility was the trace amount of AC in the formulation, but AC degradation when exposed to water, heat and light make it impossible to form conjugates or pairs (Essodolom, 2020; Tikekar et al., 2011; Dolińska, 2012; Laing et al., 2006). Additionally, the oxidation of AC increases in CS solution containing acetic acid and extensively decreases the AC stability (Zoldners et al., 2005). The bending vibrations of CH_2 -related groups in nanocomposites could be observed in the 1350–1450 cm^{-1} region. The stretching absorption bands associated with the C–O–C bridge and C–O groups also appeared in 1140–1040 cm^{-1} region (Lim and Hudson, 2004; Vino, 2012; Song, 2013).

3.3. Field emission scanning electron microscopy (FESEM)

The morphological and size studies have been performed using the FESEM images (Fig. 3). It appears that morphologically

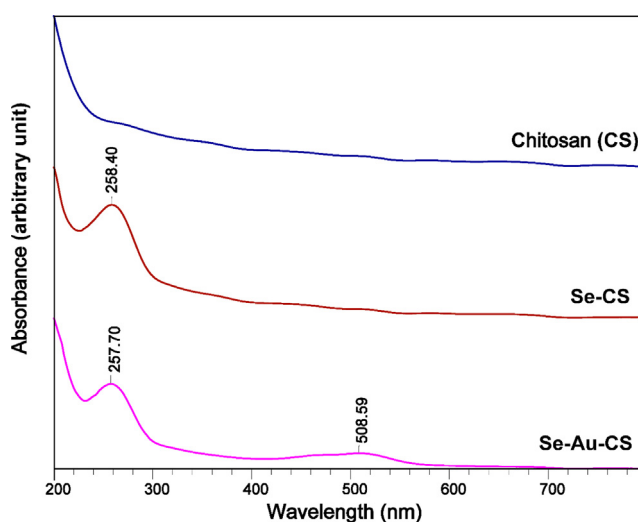


Fig. 6 The UV–Vis curves of chitosan (CS), Se-CS and Se-Au-CS.

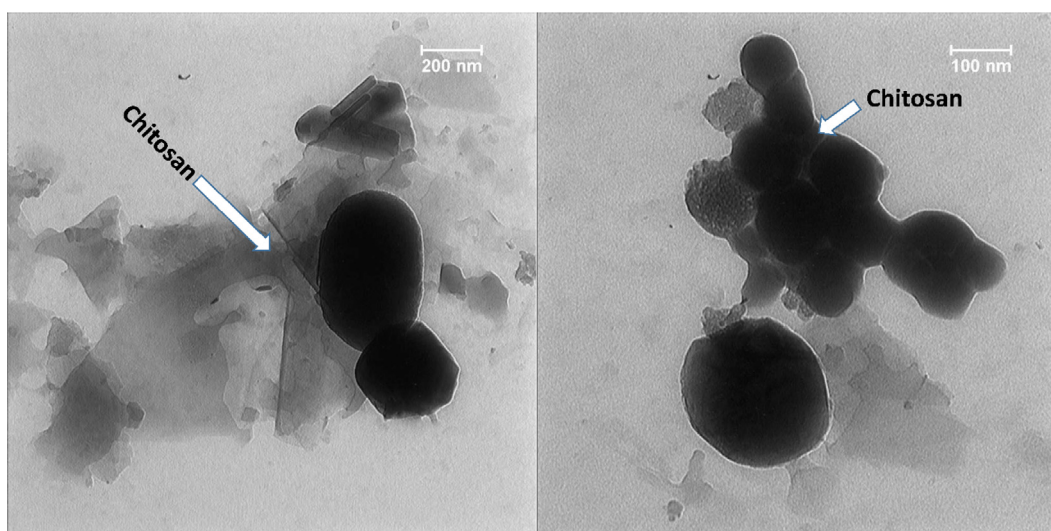


Fig. 5 TEM of the Se-Au-CS.

the particles demonstrated different polyhedral geometrical shapes from rectangle and square to some hexagonal and spherical morphologies. The prominent morphology was the rectangular and square shape, although structurally the XRD analysis revealed hexagonal crystal structures. The particle size was determined by ImageJ software (Ver. 1.53 K). The particle size distribution has displayed a mean size of approximately 211.16 nm.

The energy dispersive X-ray analysis (EDX) also shows the presence of metallic content in the Se-Au-CS (Fig. 4). The

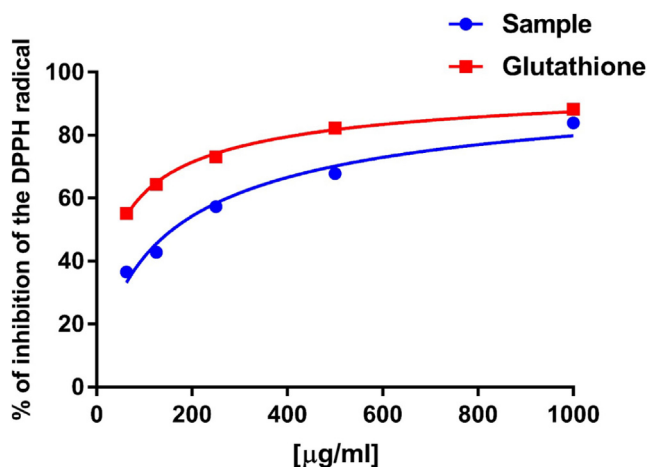


Fig. 7 The percent inhibition of DPPH free radicals in the presence of 62.5, 125, 250, 500 and 1000 $\mu\text{g/ml}$ Se-Au-CS using GSH as a positive control.

intensity of Se $L\alpha$ and Au $L\alpha$ have demonstrated the presence of 96.87% and 3.13% of metallic selenium and gold in the final structure. The EDX analysis also revealed the purity of the Se-Au-CS with no other metallic contamination.

3.4. Transmission electron microscopy (TEM)

TEM images were used for the analysis of the morphology and sizes of the nanoparticles in the CS support (Fig. 5). It appears the particles were spherical and in some cases like oval shape which were enveloped with a shell of CS and indicated the presence of agglomeration of two or more particles together. The particle sizes from TEM images conformed with the particle sizes obtained from the FESEM images and were nearly between 100 and 400 nm.

3.5. UV-Visible spectra

The UV-Vis spectra of the Chitosan (CS), Se-CS and Se-Au-CS were also taken to analyze the presence of nanoparticles in the solution (Fig. 6). To prepare the samples, the as-prepared solutions and nanoparticles were used and diluted with deionized water in order to obtain the curves. The UV-Vis spectrum of pure CS solution revealed no specific peaks (Wang, 2016). On the other hand, the appearance of the peak of selenium nanoparticles at 258 nm indicated the successful synthesis of Se-CS (Vahdati and Tohidi Moghadam, 2020). Interestingly, the peaks of 257 and 508 nm were observed in the case of Se-Au-CS, indicating the synthesis of Selenium nanoparticles as well as gold nanoparticles in order (Selvapriya, 2022; Vahdati and Tohidi Moghadam, 2020).

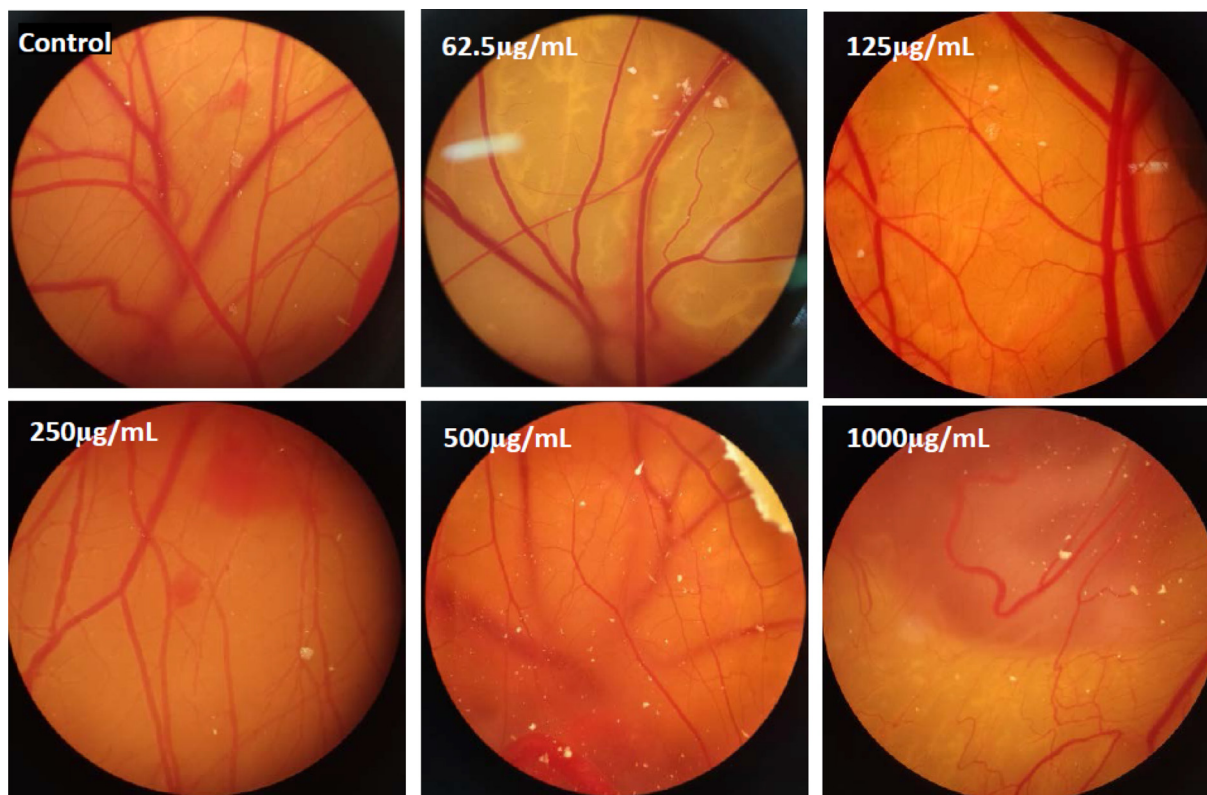


Fig. 8 Decline of angiogenesis in the samples that were exposed to various doses of Se-Au-CS compared with the control group.

3.6. DPPH free radical scavenging capacity

The DPPH method is based on its reduction in the presence of an antioxidant compound as a hydrogen donor. In this work, the inhibitory result of nanoparticles on free radicals was assessed and the results are presented in Fig. 7. IC_{50} values were recorded at about 200 $\mu\text{g}/\text{mL}$ for nanoparticles, with GSH as a positive control.

3.7. CAM assay

The CAM assay has been verified as a credible *in vivo* pattern to study angiogenesis. Several inhibitors and/or stimulators of angiogenesis have been tested using this technique (Ribatti, 2010). Morphological studies of CAM of chicken treated with different concentrations of Se-Au-CS is shown in Fig. 8.

As shown in Fig. 9, the length and number of blood vasculature have been reduced ($P < 0.05$) in the treated sample compared with the control group. Various doses of Se-Au-CS on CAM, these concentrations led to strong alterations in blood vessels. One of the major problems in approaches to combatting tumor treatment is enhancing the number and length of

blood vessels in tumors. The results of this study could be employed for antitumor drug materials.

Moreover, various studies revealed the anti-angiogenesis effect of other nanoparticles using different methods. In another study that was conducted in 2021 anti-angiogenesis effects of metformin-loaded gold-poly(catechin) core-shell nanoparticles exhibit superior anti-angiogenic properties (Luo, 2021) that are similar to our results for Se-Au-CS. Taken together, the results of this work confirmed the pharmaceutical considerable potential for Se-Au-CS and demonstrated its antioxidant and anti-angiogenesis activity.

3.8. Cytotoxicity results

Toxicology study of materials is a field of science that helps us understand the harmful properties that materials can have on humans, animals, and the environs (Sepahi, 2022; Taghavizadeh Yazdi, 2021). To assess the cell toxicity properties of the nanocomposites, diverse concentrations of NCs were added to HUVEC cells, and the cytotoxicity consequences were analyzed. The consequences revealed that the prepared nanocomposites show a very low toxic effect on HUVEC cells (Fig. 10).

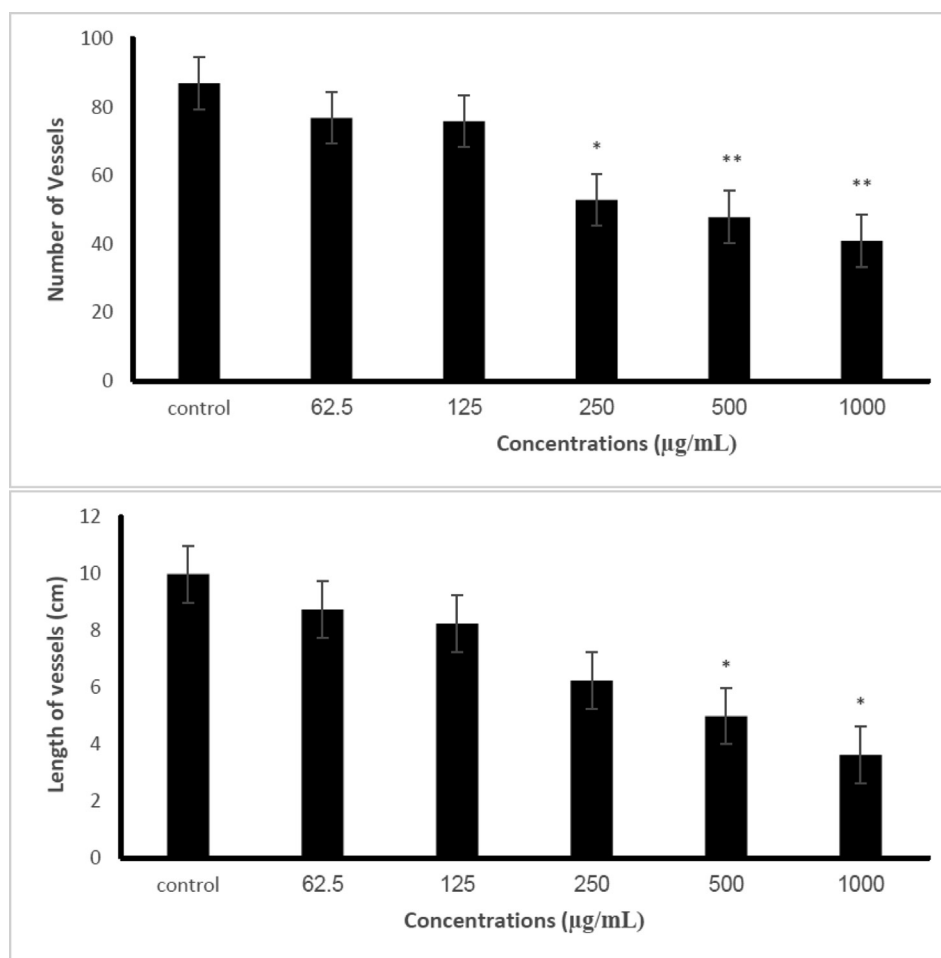


Fig. 9 The alteration of number and length vessels in the chicken chorioallantoic membrane under exposure with 0, 62.5, 125, 250, 500 and 1000 $\mu\text{g}/\text{mL}$ Se-Au-CS compared with the control sample. The results are expressed as mean \pm SD.

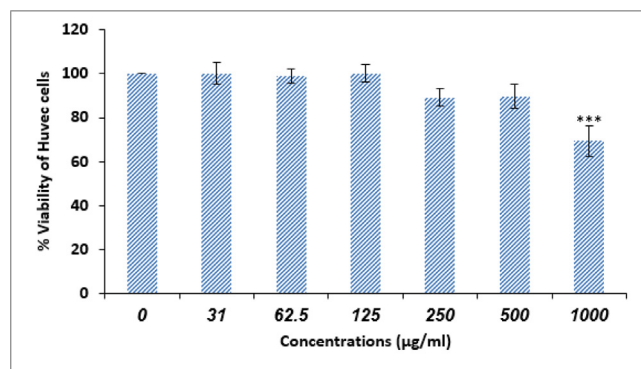


Fig 10 Cytotoxicity activity of biosynthesized Se-Au-CS.

4. Conclusion

The three-component nanocomposite of Se-Au-CS was prepared and its anticancer properties were investigated. The XRD analyses confirmed the synthesis of the. The FTIR spectrum revealed the presence of functional groups associated with CS and AC. Therefore, it can be deduced that trace amounts of AC in the structure could be due to the electrostatic interaction between CS and AC that cannot be removed. The morphological studies by TEM and FESEM also indicated the majority of particles were square-, rectangular-, polyhedral- and spherical-like shapes. The particle sizes in both TEM and FESEM images were in conformity with each other and it was found to be in the range of 100–400 nm. The mean particle size that is obtained from FESEM images was nearly 211 nm. Anti-angiogenesis effects of Se-Au-CS were evaluated using CAM assay and were shown that the number and length of the blood vessels reduced considerably in a dose/dependent way compared with the control ($p < 0.05$) group.

Declaration of Competing Interest

The authors declare that they have no known competing financial interests or personal relationships that could have appeared to influence the work reported in this paper.

Acknowledgments

The authors appreciate and acknowledge for support and assistance provided by the Islamic Azad University of Mashhad and Mashhad University of Medical Sciences.

References

- Alabyadh, T. et al, 2022. ZnO/CeO₂ nanocomposites: metal-organic framework-mediated synthesis, characterization, and estimation of cellular toxicity toward liver cancer cells. *J. Functional Biomater.* 13 (3), 139.
- Amiri, M.S., Yazdi, M.E.T., Rahnema, M., 2021. Medicinal plants and phytotherapy in Iran: glorious history, current status and future prospects. *Plant Sci. Today* 8 (1), 95–111.
- Asghar, M.A. et al, 2021. A review on toxicity and challenges in transferability of surface-functionalized metallic nanoparticles from animal models to humans. *Bio Integration* 2 (2), 71–80.
- Ashna, M. et al, 2020. Greener synthesis of cerium oxide nanoemulsion using pollen grains of *Brassica napus* and evaluation of its antitumour and cytotoxicity properties. *Mater. Technol.*, 1–8.
- Bai, K. et al, 2017. Preparation and antioxidant properties of selenium nanoparticles-loaded chitosan microspheres. *Int. J. Nanomed.* 12, 4527–4539.
- Colomer, M.T., 2013. Straightforward synthesis of Ti-doped YSZ gels by chemical modification of the precursors alkoxides. *J. Sol-Gel Sci. Technol.* 67.
- Dolińska, B. et al, 2012. Influence of trace elements on stabilization of aqueous solutions of ascorbic acid. *Biol Trace Elem Res* 150 (1–3), 509–512.
- Es-haghi, A. et al, 2021. Application of response surface methodology for optimizing the therapeutic activity of ZnO nanoparticles biosynthesized from *Aspergillus niger*. *Biomimetics* 6 (2), 34.
- Essodolom, P. et al, 2020. Effect of temperature on the degradation of ascorbic acid (vitamin c) contained in infant supplement flours during the preparation of porridges. *Int. J. Adv. Res* 8 (3), 116–121.
- Evans, S.O., Khairuddin, P.F., Jameson, M.B., 2017. Optimising selenium for modulation of cancer treatments. *Anticancer Res* 37 (12), 6497–6509.
- Forceville, X. et al, 2022. Delayed increase of plasma selenoproteins and absence of side effect induced by infusion of pharmacological dose of sodium selenite in septic shock: secondary analysis of a multicenter, randomized controlled trial. *J. Trace Elem. Med Biol.* 73, 127031.
- Frick, J. et al, 2021. Impact of acid type and glutaraldehyde crosslinking in the physicochemical and mechanical properties and biodegradability of chitosan films. *Polym. Bull.* 78.
- Ghorani-Azam, A. et al, 2022. Resveratrol-Mediated gold-nanoceria synthesis as green nanomedicine for phytotherapy of hepatocellular carcinoma. *Front. Biosci.-Landmark* 27 (8), 227.
- Hashemzadeh, M.R. et al, 2021. Stem cell therapy in the heart: biomaterials as a key route. *Tissue Cell* 101504.
- Hashemzadeh, A. et al, 2022. Sulfasalazine colon-specific drug delivery by selenium nanoparticle. *J. Trace Elements Minerals* 2, 100012.
- Hojjati Fard, F. et al, 2022. Nanoselenium improved learning, memory, and brain-derived neurotrophic factor and attenuated nitric oxide, and oxidative stress in the brain of juvenile hypothyroid rats. *Metab. Brain Dis.* 37 (8), 2719–2733.
- Javad Farhangi, M. et al, 2021. MOF-Mediated Synthesis of CuO/CeO₂ composite nanoparticles: characterization and estimation of the cellular toxicity against breast cancer cell line (MCF-7). *J. Functional Biomater.* 12 (4), 53.
- Julkapli, N.M., Ahmad, Z., Akil, H.M., X-Ray diffraction studies of cross linked chitosan with different cross linking agents for waste water treatment application. In: AIP conference proceedings, 2010. American Institute of Physics.
- Jurj, A. et al, 2017. The new era of nanotechnology, an alternative to change cancer treatment. *Drug Des. Devel. Ther.* 11, 2871.
- Kang, M.S. et al, 2020. State of the art biocompatible gold nanoparticles for cancer theragnosis. *Pharmaceutics* 12 (8), 701.
- Labunskyy, V.M., Hatfield, D.L., Gladyshev, V.N., 2014. Selenoproteins: molecular pathways and physiological roles. *Physiol. Rev.* 94 (3), 739–777.
- Lai, P.-X. et al, 2016. Ultrastrong trapping of VEGF by graphene oxide: anti-angiogenesis application. *Biomaterials* 109, 12–22.
- Laing, B., Schlueter, D., Labuza, T., 2006. Degradation kinetics of ascorbic acid at high temperature and water activity. *J. Food Sci.* 43, 1440–1443.
- Lim, S.-H., Hudson, S.M., 2004. Synthesis and antimicrobial activity of a water-soluble chitosan derivative with a fiber-reactive group. *Carbohydr. Res.* 339 (2), 313–319.
- Luo, L.-J. et al, 2021. Targeting nanocomposites with anti-oxidative/inflammatory/angiogenic activities for synergistically alleviating macular degeneration. *Appl. Mater. Today* 24, 101156.
- Malinga, T., Kudanga, T., Mbatha, L.S., 2021. Stealth doxorubicin conjugated bimetallic selenium/silver nanoparticles for targeted cervical cancer therapy. *Adv. Nat. Sci. Nanosci. Nanotechnol.* 12, (4) 045006.
- Mangiapan, E., Pessione, A., Pessione, E., 2014. Selenium and selenoproteins: an overview on different biological systems. *Curr. Protein Pept. Sci.* 15 (6), 598–607.

- Mirzaei, S.Z. et al, 2021. Phyco-fabrication of bimetallic nanoparticles (zinc-selenium) using aqueous extract of *Gracilaria corticata* and its biological activity potentials. *Ceram. Int.* 47 (4), 5580–5586.
- Mobaraki, F. et al, 2021. Plant-derived synthesis and characterization of gold nanoparticles: Investigation of its antioxidant and anti-cancer activity against human testicular embryonic carcinoma stem cells. *Process Biochem.* 111, 167–177.
- Mobaraki, F. et al, 2022. Apoptotic, antioxidant and cytotoxic properties of synthesized AgNPs using green tea against human testicular embryonic cancer stem cells. *Process Biochem.*
- Modarres, M., Yazdi, M.E.T., 2021. Elicitation improves phenolic acid content and antioxidant enzymes activity in *salvia leriifolia* cell cultures. *Iranian J. Sci. Technol. Trans. A Sci.*, 1–7
- Mohamed, A.S. et al, 2021. Silver/chitosan nanocomposites induce physiological and histological changes in freshwater bivalve. *J. Trace Elem. Med Biol.* 65, 126719.
- Mohammadzadeh, V. et al, 2022. Applications of plant-based nanoparticles in nanomedicine: a review. *Sustain. Chem. Pharm.* 25, 100606.
- Mousavi-Kouhi, S.M. et al, 2021. Silver-zinc oxide nanocomposite: from synthesis to antimicrobial and anticancer properties. *Ceram. Int.* 47 (15), 21490–21497.
- Mousavi-Kouhi, S.M. et al, 2021. Biological synthesis and characterization of gold nanoparticles using *Verbascum speciosum* Schrad. and cytotoxicity properties toward HepG2 cancer cell line. *Res. Chem. Intermed.*, 1–12
- Phan, T.T.V. et al, 2021. Roles of chitosan in green synthesis of metal nanoparticles for biomedical applications. *Nanomaterials (Basel)* 11 (2).
- Qi, L. et al, 2022. The role of selenoprotein p in the determining the sensitivity of cervical cancer patients to concurrent chemoradiotherapy: a metabonomics-based analysis. *J. Trace Elem. Med Biol.* 127041
- Radomska, D. et al, 2021. Selenium as a bioactive micronutrient in the human diet and its cancer chemopreventive activity. *Nutrients* 13 (5), 1649.
- Raich, P.C. et al, 2001. Selenium in cancer prevention: clinical issues and implications. *Cancer Invest.* 19 (5), 540–553.
- Rajamanikandan, S. et al, 2011. Radical scavenging and antioxidant activity of ethanolic extract of *Mollugo nudicaulis* by invitro assays. *Indian J. Pharm. Educat. Res.* 45 (4), 310–316.
- Rana, T., 2021. Prospects and future perspectives of selenium nanoparticles: an insight of growth promoter, antioxidant and anti-bacterial potentials in productivity of poultry. *J. Trace Elem. Med Biol.* 68, 126862.
- Rataan, A.O. et al, 2022. Potential role of selenium in the treatment of cancer and viral infections. *Int. J. Mol. Sci.* 23 (4), 2215.
- Ribatti, D., 2010. The chick embryo chorioallantoic membrane as an in vivo assay to study antiangiogenesis. *Pharmaceuticals* 3 (3), 482–513.
- Selvapriya, R. et al, 2022. Fabrication of bimetallic inlaid working electrode for highly efficient dye sensitized solar cells. *J. Alloy. Compd.* 939, 168634.
- Seol, S.K. et al, 2013. One-Step synthesis of PEG-coated gold nanoparticles by rapid microwave heating. *J. Nanomater.* 2013.
- Sepahi, S. et al, 2022. Biochemical responses as early and reliable biomarkers of organophosphate and carbamate pesticides intoxication: a systematic literature review. *J. Biochem. Mol. Toxicol.*, e23285
- Seyedi, Z. et al, 2023. Icaritin: a promising natural product in biomedicine and tissue engineering. *J. Functional Biomater.* 14 (1), 44.
- Shakerimanes, K. et al, 2022. Biomimetic synthesis and characterization of homogenous gold nanoparticles and estimation of its cytotoxicity against breast cancer cell line. *Mater. Technol.*, 1–8
- Singh, J., Dutta, P., 2009. Preparation, circular dichroism induced helical conformation and optical property of chitosan acid salt complexes for biomedical applications. *Int. J. Biol. Macromol.* 45 (4), 384–392.
- Song, C. et al, 2013. Physicochemical properties and antioxidant activity of chitosan from the blowfly *Chrysomya megacephala* larvae. *Int. J. Biol. Macromol.* 60, 347–354.
- Taghavizadeh Yazdi, M.E. et al, 2021. Bio-indicators in cadmium toxicity: Role of HSP27 and HSP70. *Environ. Sci. Pollut. Res.* 28 (21), 26359–26379.
- Taghavizadeh Yazdi, M.E. et al, 2022. Antimycobacterial, anticancer, antioxidant and photocatalytic activity of biosynthesized silver nanoparticles using *Berberis Integerrima*. *Iranian J. Sci. Technol. Trans. A: Sci.* 46 (1), 1–11.
- Teleanu, R.I. et al, 2019. Tumor angiogenesis and anti-angiogenic strategies for cancer treatment. *J. Clin. Med.* 9 (1), 84.
- Tikekar, R.V., Anantheswaran, R.C., LaBorde, L.F., 2011. Ascorbic acid degradation in a model apple juice system and in apple juice during ultraviolet processing and storage. *J Food Sci* 76 (2), H62–H71.
- Vahdati, M., Tohidi Moghadam, T., 2020. Synthesis and characterization of selenium nanoparticles-lysozyme nanohybrid system with synergistic antibacterial properties. *Sci. Rep.* 10 (1), 510.
- Vino, A.B. et al, 2012. Extraction, characterization and in vitro antioxidative potential of chitosan and sulfated chitosan from Cuttlebone of *Sepia aculeata* Orbigny, 1848. *Asian Pac. J. Trop. Biomed.* 2 (1), S334–S341.
- Wang, Y. et al, 2016. Nanoparticles of chitosan conjugated to organo-ruthenium complexes. *Inorg. Chem. Front.* 3 (8), 1058–1064.
- Yazdi, M.E., Amiri, M.S., Darroudi, M., 2020. Biopolymers in the Synthesis of Different Nanostructures.
- Zoldners, J., Kiseleva, T., Kaiminsh, I., 2005. Influence of ascorbic acid on the stability of chitosan solutions. *Carbohydr. Polym.* 60 (2), 215–218.